Acta Cryst B
STRUCTURAL SCIENCE
CRYSTAL ENGINEERING
MATERIALS

ISSN 2052-5206

# Introducing the special issue on current research in crystal growth and related characterization

**Matias Velazquez,[a]* Geetha Balakrishnan[b] and Tatyana B. Bekker[c]**

[a]Université Grenoble Alpes, CNRS, Grenoble INP (Institute of Engineering, Université Grenoble Alpes), SIMAP, 38000 Grenoble France, [b]Department of Physics, University of Warwick, Coventry CV4 7AL, United Kingdom, and [c]Institute of Geology and Mineralogy, Novosibirsk, Russian Federation. *Correspondence e-mail: matias.velazquez@grenoble-inp.fr

**Keywords:** crystal growth; bulk crystals; structure–property relationships; functional materials; anisotropy; metastability.

The discovery of the optical and mechanical properties of natural calcite and quartz crystals led to the study of scientific crystallography, as a discipline, in the 18th century. What eventually followed during the 20th century was a rather serious and urgent pursuit for zero defect (or defect-free) silicon crystals for microelectronics, which placed the research on crystal growth firmly on the materials science and related R&D maps. Since then, at least two drivers have consistently motivated crystal growers around the world: (i) the search for and growth of new categories of bulk crystals with challenging thermodynamic properties, and (ii) to the production of already studied and established 'functional' crystals more quickly and more cheaply, with enhanced/optimum quality in the large sizes required for applications. The reasons behind these drivers are that not only do single crystals allow us to investigate the intrinsic properties of crystalline matter, the most fundamental one being the average crystal structure, but they also allow us to study and exploit the anisotropy exhibited in their physical properties, to test fundamental theories and to develop new and/or improve existing technologies.

The articles collected for this special issue in *Acta Crystallographica Section B* illustrate these points above and encapsulate the current status of the literature on a few chosen important material categories. The readers will indeed find articles where the resolution of complex crystal structures is presented, the crystal growth of hitherto unavailable single crystals reported, as well as the development of well-known single crystals of bigger sizes and the investigations of their properties, including, of course, their most salient anisotropic features.

Starting with oxides, Vladimir A. Morozov *et al.* (2026) use synchrotron powder X-ray diffraction (XRD) data to resolve (3+1)D-modulated monoclinic $M_{1/8}Pr_{5/8}\square_{1/4}MoO_4$ ($M$ = Li, Na, K; □ = cation vacancy) scheelite structures, synthesized by solid state reactions. An antiphase relation of the occupancy modulation waves for $Li^+/Na^+$ and $Pr^{3+}$ atoms was found. In all cases, the modulation arises from ordering of $M^+/Pr^{3+}$ cations and cation vacancies at the $A$-sublattice of the parent scheelite $ABO_4$ structure.

Christo Guguschev *et al.* (2026) describe a study of floating-zone grown 5N-purity and crack-free MgO substrate single crystals, a highly refractory material that is particularly difficult to obtain with diameters between 3.5 and 5 mm and lengths up to 40 mm. To circumvent the problems arising from their extreme thermodynamic properties, high growth rates between 35 and 50 mm $h^{-1}$, high $Ar/O_2$ gas mixture flow and high axial temperature gradients ~225 K $mm^{-1}$ have been used, which eventually led to crystal purities one order of magnitude higher than the state-of-the-art commercial ones.

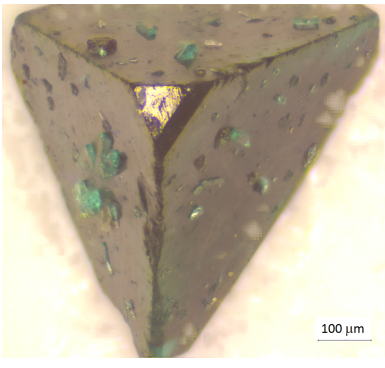


In the same field of oxide crystals for substrate manufacturing, Roberts Blukis *et al.* (2026) investigate (Nd,Sr)(Al,Ta)$O_3$ (NSAT) solid-solution crystals using powder and single-crystal XRD, transmission electron microscopy, infrared (IR) and ultraviolet–visible range ellipsometry as well as IR and Raman spectroscopies. While the average cubic perovskite unit cell has parameter $a$ = 3.8427 Å, right in the lattice constant range for which no other satisfactory oxide perovskite substrate is known, Al/Ta superstructure ordered nanoscale domains with a doubled unit-cell parameter are observed. The implications for the use of NSAT as a substrate for the growth of perovskite and perovskite-related films and strain engineering are discussed.

$LiNiO_2$ is another crystal which has been successfully grown for the first time by the optical floating-zone technique by Uthayakumar Sivaperumal *et al.* (2026). Single-crystal XRD allowed them to establish its crystal structure and to unveil superstructures and

electronic ordering in its bulk form as a function of temperature. Combined with synchrotron X-ray and resonant elastic X-ray scattering, the mixed valence states of different Ni sites associated with superlattice reflections are shown.

In their contribution to this special issue, Grigorieva *et al.* (2026) address a challenge in crystal growth: the tendency of $Li_2WO_4$ to undergo destructive phase transitions. They successfully grow high-quality, large-diameter crystals using the low-temperature-gradient Czochralski technique. They show that even minimal molybdenum substitution (down to 1.25 mol%) stabilizes the trigonal structure and completely suppresses phase transitions. Their systematic study of the modified luminescence properties, combined with the demonstration of X-ray-excited emission, confirms $Li_2WO_4$ as a promising scintillator for rare-event physics.

Krzhizhanovskaya *et al.* (2026) investigate the link between negative thermal expansion (NTE) and high-temperature luminescence in Ho,Tm-doped $Yb_2Mo_3O_{12}$ crystals. Using *in situ* single-crystal XRD from 100 K to 1273 K, they show that the orthorhombic phase exhibits strong NTE up to 1173 K due to angular deformation of the polyhedral framework, not changes in bond lengths. As temperature increases, the 655 nm emission band shows two plateau regions (570–650 K and 700–800 K) where its intensity remains nearly constant, while a new 700 nm emission appears via phonon activation. The opposite temperature responses of the 655 nm and 700 nm bands enable a ratiometric optical thermometer with 0.4 K resolution.

Sergei Naydenov *et al.* (2026) report, for the first time, the growth of triple-doped (Cr,Co,Fe):ZnSe single crystals by the vertical Bridgman method under high argon pressure. The key novelty is the successful incorporation of three transition-metal activators simultaneously into the ZnSe lattice, enabling controlled energy transfer for mid-infrared laser operation in the 2–5 µm range. Cobalt is shown to incorporate with unusually high efficiency due to its ionic radius matching that of $Zn^{2+}$, while the spatial distribution of all three dopants remains remarkably uniform throughout the crystal volume – a critical requirement for practical laser elements. The overlapping $Cr^{2+}$ and $Co^{2+}$ absorption bands form a composite maximum near 1.71 µm, whereas the $Fe^{2+}$ band near 3 µm stays unchanged, providing a spectroscopic basis for designing multi-activated laser media.

In the realm of intermetallics endowed with remarkable properties, Daniel A. Mayoh *et al.* (2026) report a systematic study of the structural and magnetic evolution in Weyl semimetals $CeAlSi_{1-x}Ge_x$ ($x$ = 0.0–1.0), a series of materials which provide a tunable platform for exploring magnetism in noncentrosymmetric Ce-based intermetallics. Here, polycrystalline samples and single crystals are synthesized using arc melting and flux growth techniques. The effect of substituting Ge on the Si site was examined using powder XRD, which revealed an expansion of the unit-cell parameters with no observable change in the crystal structure across the series. Magnetization measurements reveal a suppression of the ferromagnetic ordering temperature of CeAlSi with increasing Ge substitution, indicating a crossover toward antiferromagnetic behaviour in Ge-rich compositions. Powder neutron diffraction data collected on $CeAlSi_{0.7}Ge_{0.3}$ and $CeAlSi_{0.3}Ge_{0.7}$ show a nuclear structure consistent with tetragonal space group $I4_1md$, with weak magnetic peaks observed below the magnetic transition temperature of $CeAlSi_{0.3}Ge_{0.7}$.

Courac & Le Godec (2026) provide a critical review of metastable silicon allotropes synthesized under high-pressure–high-temperature conditions, combining original crystallographic observations with a systematic analysis of phase transformation mechanisms. Using *in situ* XRD and large-volume press techniques, they examine both dense phases (Si-II, Si-III, Si-XI) and open-framework clathrates ($Si_{24}$,$Si_{136}$) obtained from Na–Si systems. The authors demonstrate that phase transitions are governed by the interplay of thermodynamics, kinetics, and shear stress, and they clarify the crystallographic nature of hexagonal Si-IV polytypes, showing that Si-III transforms into the 4H form, which can further convert to a 6H polytype upon thermal treatment in vacuum, a phase previously suggested only as a crystallographic curiosity. By critically reassessing claimed but irreproducible phases (Si-VIII, Si-IX) and integrating experimental data with computational modeling, this work establishes a framework linking crystal growth pathways, structural metastability, and functional properties of silicon allotropes.

Anassya Raad *et al.* (2026) perform a quantitative analysis of facet growth during directional solidification of salol, a transparent model material very useful in investigations aimed at understanding the formation of structures in faceted materials. The study reveals that after an initial transient period, the solid–liquid interface stabilizes, with its position linked to the interface undercooling, which in turn is related to the growth mechanism. Facet size heterogeneity is characterized by a tendency to form larger facets for lower temperature gradients. A methodology is developed to exploit experimentally measured angles into a three-dimensional angle in the crystals, allowing the identification of the crystallographic nature of the facets. The analysis of facet velocities as a function of undercooling suggests a growth mechanism primarily controlled by two-dimensional nucleation. Thanks to these experiments, factors influencing facet behaviour, growth, and orientation are explored. It is expected that the methodologies developed in this work will eventually lead to further investigations and have potential applications in studying other systems.

This special issue also addresses biological crystallization, as exemplified by the work of Thierry Prangé *et al.* (2025), who were able to design a clever cyclic and slow temperature cooling technique to obtain good quality needle-like flocculosin-A crystals with a maximum thickness of 5 mm and several millimetres long. Its structure was solved using XRD, which makes it possible to determine by comparison the absolute configuration of the asymmetric C atoms of the lipid chains attached to the cellobiose moiety of the molecule.

Liang *et al.* (2026) extend the crystalline mate strategy to ionic natural products, obtaining two co-crystals of berberine

hydrochloride with the $Ag_3Pz_3$ complex. Solvent polarity determines the outcome: without protic solvents, a chloride-bridged sandwich structure (SF) forms that also binds the berberine cation. When methanol or ethanol is present, a second form (NSF) appears, in which chloride is absent and $Ag_3Pz_3$ reorganizes into a rare anionic $Ag_3Pz_4$ cluster that serves as a counterion.

Analeece Long *et al.* (2026) report the first accurate low-temperature single-crystal structures of several Maus's salts, including the parent compound originally discovered nearly 200 years ago. The key novelty lies in resolving longstanding ambiguities of these highly solvated and dehydration-sensitive iron sulfates. The parent salt reveals a trigonal arrangement of $Fe^{3+}$ trimers that enables possible magnetic frustration, while the substitution of larger caesium unexpectedly yields an entirely different structure based on $Fe^{3+}$ tetramers instead of the classical Maus's salt motif. Preliminary magnetic data suggest a splayed spin configuration within the trimers, opening a pathway to frustrated magnetism in this ancient family of compounds.

Xing-Zhong Li (2026) offers a description of *CRYSP*, a user-friendly software that permits the construction and visualization of crystal shapes in natural habits and on planar substrates, by means of an improved Wulff construction algorithm that includes a cleavage option, enabling the identification of very small facets, short edges, and nearly coincidence vertices. This application extends to the shapes associated with non-crystallographic point groups. Overall, it is a useful tool for crystallography, nanostructures, and any other field where crystal facets play a vital role.

## References


Blukis, R., Rhode, C., Remmele, T., Kluth, E., Goldhahn, R., Feneberg, M., Celotto, A., Divitini, G., Brützam, M., Schlom, D. G. & Guguschev, C. (2026). *Acta Cryst.* B**82**, 131–142.

Courac, A. & Le Godec, Y. (2026). *Acta Cryst.* B**82**, 280–298.

Grigorieva, V. D., Bazanova, E. D., Artemyeva, M. A., Balyan, L. A., Khramtsova, D. M., Yelisseyev, A. P., Rakhmanova, M. I., Musikhin, A. E., Kuznetsov, A. B. & Shlegel, V. N. (2026). *Acta Cryst.* B**82**, 258–267.

Guguschev, C., Schulze, M., Dittmar, A., Klimm, D., Dadzis, K., Schroeder, T., Peters, K. & Pushp, A. (2026). *Acta Cryst.* B**82**, 2–13.

Krzhizhanovskaya, M. G., Povolotskiy, A. V., Maltsev, V. V., Volkova, E. A., Koporulina, E. V., Bubnova, R. S. & Filatov, S. K. (2026). *Acta Cryst.* B**82**, 165–174.

Li, X.-Z. (2026). *Acta Cryst.* B**82**, 14–21.

Liang, J.-F., Wang, Y.-T., Xie, M. & Li, D. (2026). *Acta Cryst.* B**82**, 159–164.

Long, A., Powell, M., Dickey, A., McMillen, C. & Kolis, J. (2026). *Acta Cryst.* B**82**, 268–279.

Mayoh, D. A., Sharma, S., Chamberlain, T. W., Wood, G. D. A., da-Silva, I., Goddard, P. A., Lees, M. R. & Balakrishnan, G. (2026). *Acta Cryst.* B**82**, 250–257.

Morozov, V. A., Deyneko, D. V., Filatova, D. G., Belik, A. A., Basovich, O. M., Khaikina, E. G. & Lazoryak, B. I. (2026). *Acta Cryst.* B**82**, 120–130.

Naydenov, S., Kapustnyk, O., Pritula, I. & Sofronov, D. (2026). *Acta Cryst.* B**82**, 112–119.

Prangé, T., Nam Phan, G., Shepard, W., Ponchet, M., Lapeyre, L. & Mehiri, M. (2025). *Acta Cryst.* B**81**, 502–505.

Raad, A., Bergeon, N., Mangelinck-Noël, N. & Mota, F. L. (2026). *Acta Cryst.* B**82**, 143–153.

Sivaperumal, U., Porter, D. G., Voneshen, D. J. & Goff, J. P. (2026). *Acta Cryst.* B**82**, 154–158.